Multimodal characterization of compositional, structural and functional features of human atherosclerotic plaques

Yang Sun,[1] Abhijit J. Chaudhari,[2] Matthew Lam,[1] Hongtao Xie,[1] Diego R. Yankelevich,[3] Jennifer Phipps,[1] Jing Liu,[1] Michael C. Fishbein,[4] Jonathan M. Cannata,[5] K. Kirk Shung,[5] and Laura Marcu[1,*]

[1]*University of California, Davis, Department of Biomedical Engineering, 451 Health Sciences Drive, Davis, California 95616, USA*

[2]*University of California, Davis School of Medicine, Department of Radiology, 4860 Y Street, Sacramento, California 95817, USA*

[3]*University of California, Davis, Department of Electrical and Computer Engineering, One shields Avenue, Davis, California 95616, USA*

[4]*University of California, Los Angeles, Department of Pathology, 10833 Le Conte Ave, Los Angeles, California 90095, USA*

[5]*University of Southern California, Department of Biomedical Engineering, 1042 Downey way, DRB 140, Los Angeles, California 90089, USA*

**lmarcu@ucdavis.edu*

Abstract: Detection of atherosclerotic plaque vulnerability has critical clinical implications for avoiding sudden death in patients with high risk of plaque rupture. We report on multimodality imaging of ex-vivo human carotid plaque samples using a system that integrates fluorescence lifetime imaging (FLIM), ultrasonic backscatter microscopy (UBM), and photoacoustic imaging (PAI). Biochemical composition is differentiated with a high temporal resolution and sensitivity at the surface of the plaque by the FLIM subsystem. 3D microanatomy of the whole plaque is reconstructed by the UBM. Functional imaging associated with optical absorption contrast is evaluated from the PAI component. Simultaneous recordings of the optical, ultrasonic, and photoacoustic data present a wealth of complementary information concerning the plaque composition, structure, and function that are related to plaque vulnerability. This approach is expected to improve our ability to study atherosclerotic plaques. The multimodal system presented here can be translated into a catheter based intraluminal system for future clinical studies.

OCIS codes: (170.6510) Spectroscopy, tissue diagnostics; (300.6500) Spectroscopy, time-resolved; (110.7170) Ultrasound; (170.5120) Photoacoustic imaging; (170.6935) Tissue characterization.

References and links

1. P. Libby, "Inflammation in atherosclerosis," Nature **420**(6917), 868–874 (2002).
2. I. K. Jang, B. E. Bouma, D. H. Kang, S. J. Park, S. W. Park, K. B. Seung, K. B. Choi, M. Shishkov, K. Schlendorf, E. Pomerantsev, S. L. Houser, H. T. Aretz, and G. J. Tearney, "Visualization of coronary atherosclerotic plaques in patients using optical coherence tomography: comparison with intravascular ultrasound," J. Am. Coll. Cardiol. **39**(4), 604–609 (2002).
3. N. Komiyama, G. J. Berry, M. L. Kolz, A. Oshima, J. A. Metz, P. Preuss, A. F. Brisken, M. P. Moore, P. G. Yock, and P. J. Fitzgerald, "Tissue characterization of atherosclerotic plaques by intravascular ultrasound radiofrequency signal analysis: an in vitro study of human coronary arteries," Am. Heart J. **140**(4), 565–574 (2000).
4. R. Richards-Kortum and E. M. Sevick-Muraca, "Quantitative optical spectroscopy for tissue diagnosis," Annu. Rev. Phys. Chem. **47**(1), 555–606 (1996).

#146656 - $15.00 USD Received 2 May 2011; revised 14 Jul 2011; accepted 14 Jul 2011; published 19 Jul 2011

5. L. Marcu, Q. Fang, J. A. Jo, T. Papaioannou, A. Dorafshar, T. Reil, J. H. Qiao, J. D. Baker, J. A. Freischlag, and M. C. Fishbein, "In vivo detection of macrophages in a rabbit atherosclerotic model by time-resolved laser-induced fluorescence spectroscopy," Atherosclerosis **181**(2), 295–303 (2005).
6. L. V. Wang, "Tutorial on photoacoustic microscopy and computed tomography," IEEE J. Sel. Top. Quantum Electron. **14**(1), 171–179 (2008).
7. R. Virmani, A. P. Burke, A. Farb, and F. D. Kolodgie, "Pathology of the vulnerable plaque," J. Am. Coll. Cardiol. **47**(8 Suppl), C13–C18 (2006).
8. D. S. Elson, J. A. Jo, and L. Marcu, "Miniaturized side-viewing imaging probe for fluorescence lifetime imaging (FLIM): validation with fluorescence dyes, tissue structural proteins and tissue specimens," N. J. Phys. **9**(127), 1–13 (2007).
9. J. Phipps, Y. H. Sun, R. Saroufeem, N. Hatami, and L. Marcu, "Fluorescence lifetime imaging microscopy for the characterization of atherosclerotic plaques," Proc. Soc. Photo Opt. Instrum. Eng. **7161**, 71612G (2009).
10. Y. Sun, J. Park, D. N. Stephens, J. A. Jo, L. Sun, J. M. Cannata, R. M. Saroufeem, K. K. Shung, and L. Marcu, "Development of a dual-modal tissue diagnostic system combining time-resolved fluorescence spectroscopy and ultrasonic backscatter microscopy," Rev. Sci. Instrum. **80**(6), 065104 (2009).
11. J. Yuan, S. Rhee, and X. N. Jiang, "60 MHz PMN-PT based 1-3 composite transducer for IVUS imaging," *Proc. IEEE IUS*, 682–685 (2008).
12. B. Wang, J. L. Su, J. Amirian, S. H. Litovsky, R. Smalling, and S. Emelianov, "Detection of lipid in atherosclerotic vessels using ultrasound-guided spectroscopic intravascular photoacoustic imaging," Opt. Express **18**(5), 4889–4897 (2010).
13. D. N. Stephens, J. Park, Y. Sun, T. Papaioannou, and L. Marcu, "Intraluminal fluorescence spectroscopy catheter with ultrasound guidance," J. Biomed. Opt. **14**(3), 030505 (2009).
14. A. B. Karpiouk, B. Wang, and S. Y. Emelianov, "Development of a catheter for combined intravascular ultrasound and photoacoustic imaging," Rev. Sci. Instrum. **81**(1), 014901 (2010).
15. Y. H. Sun, R. Liu, D. S. Elson, C. W. Hollars, J. A. Jo, J. Park, Y. Sun, and L. Marcu, "Simultaneous time- and wavelength-resolved fluorescence spectroscopy for near real-time tissue diagnosis," Opt. Lett. **33**(6), 630–632 (2008).
16. Y. H. Sun, Y. Sun, D. Stephens, H. Xie, J. Phipps, R. Saroufeem, J. Southard, D. S. Elson, and L. Marcu, "Dynamic tissue analysis using time- and wavelength-resolved fluorescence spectroscopy for atherosclerosis diagnosis," Opt. Express **19**(5), 3890–3901 (2011).
17. J. M. Cannata, T. A. Ritter, W. H. Chen, R. H. Silverman, and K. K. Shung, "Design of efficient, broadband single-element (20-80 MHz) ultrasonic transducers for medical imaging applications," IEEE Trans. Ultrason. Ferroelectr. Freq. Control **50**(11), 1548–1557 (2003).
18. J. A. Jo, Q. Fang, T. Papaioannou, J. D. Baker, A. H. Dorafshar, T. Reil, J. H. Qiao, M. C. Fishbein, J. A. Freischlag, and L. Marcu, "Laguerre-based method for analysis of time-resolved fluorescence data: application to in-vivo characterization and diagnosis of atherosclerotic lesions," J. Biomed. Opt. **11**(2), 021004 (2006).
19. Y. H. Sun, J. Phipps, D. S. Elson, H. Stoy, S. Tinling, J. Meier, B. Poirier, F. S. Chuang, D. G. Farwell, and L. Marcu, "Fluorescence lifetime imaging microscopy: in vivo application to diagnosis of oral carcinoma," Opt. Lett. **34**(13), 2081–2083 (2009).
20. Y. Sun, J. E. Phipps, M. Lam, H. Xie, M. C. Fishbein, J. M. Cannata, K. Kirk Shung, and L. Marcu, "Characterization of atherosclerotic plaques using combined time-resolved fluorescence spectroscopy and ultrasonic backscatter microscopy," *SPIE*, 7883D–83, San Francisco, CA (2011).
21. S. Y. Emelianov, S. R. Aglyamov, A. B. Karpiouk, S. Mallidi, S. Park, S. Sethuraman, J. Shah, R. W. Smalling, J. M. Rubin, and W. G. Scott, "Synergy and applications of combined ultrasound, elasticity, and photoacoustic imaging," Proc. of IEEE Ultrasonics Symposium, 405–415 (2006).
22. C. Studholme, D. L. G. Hill, and D. J. Hawkes, "An overlap invariant entropy measure of 3D medical image alignment," Pattern Recognit. **32**(1), 71–86 (1999).
23. L. Marcu, J. A. Jo, Q. Fang, T. Papaioannou, T. Reil, J. H. Qiao, J. D. Baker, J. A. Freischlag, and M. C. Fishbein, "Detection of rupture-prone atherosclerotic plaques by time-resolved laser-induced fluorescence spectroscopy," Atherosclerosis **204**(1), 156–164 (2009).
24. L. Marcu, W. S. Grundfest, and M. C. Fishbein, "Time-resolved laser-induced fluorescence spectroscopy for staging atherosclerotic lesions," *Handbook of Biomedical Fluorescence* **12**, 397–430 (2003).
25. L. Marcu, J. A. Jo, Q. Fang, T. Papaloannou, J. H. Qiao, M. C. Fishbein, J. D. Baker, and J. A. Freischlag, "Detection of high-risk atherosclerotic plaques by time-resolved laser induced fluorescence spectroscopy," Circulation **112**, U678 (2005).
26. S. Sathyanarayana, S. Carlier, W. Li, and L. Thomas, "Characterisation of atherosclerotic plaque by spectral similarity of radiofrequency intravascular ultrasound signals," EuroIntervention **5**(1), 133–139 (2009).
27. S. Sethuraman, J. H. Amirian, S. H. Litovsky, R. W. Smalling, and S. Y. Emelianov, "Ex vivo characterization of atherosclerosis using intravascular photoacoustic imaging," Opt. Express **15**(25), 16657–16666 (2007).
28. H. Xie, J. Bec, Y. Sun, and L. Marcu, "Development of an intravascular diagnostic system integrating an IVUS-guided rotational fiber optics catheter for time-resolved fluorescence spectroscopy," 7890–15, *SPIE*, San Francisco, CA (2011).

#146656 - $15.00 USD Received 2 May 2011; revised 14 Jul 2011; accepted 14 Jul 2011; published 19 Jul 2011

1. Introduction

Atherosclerotic cardiovascular disease (ACVD), a progressive disease of arteries, is one of the major causes of death worldwide [1]. Current techniques for investigation of atherosclerotic plaques include angiography, intravascular magnetic resonance imaging (MRI), optical coherence tomography (OCT) [2], intravascular ultrasound (IVUS) [3], optical spectroscopy (NIR, Raman, and fluorescence spectroscopy) [4,5], and photoacoustic imaging (PAI) [6]. However, a single imaging technique can only provide an incomplete characterization of the lesion. More complete information concerning various markers involved in plaque vulnerability and rupture is needed for improving plaque evaluation [7]. Typically these markers encompass diverse features derived from plaque structure, composition, and function (e.g. thinning of the fibrous cap, large lipid-rich pool, macrophage presence and activity within fibrotic cap, and outward remodeling).

This pilot study investigates whether compositional, structural, and functional characteristics of human atherosclerotic plaques can be evaluated concurrently via a flexible scanning probe composed of a single fiber-optic and a single-element high-frequency ultrasonic transducer. This configuration facilitates integration of three distinct diagnostic modalities: fluorescence lifetime imaging (FLIM), ultrasonic backscatter microscopy (UBM), and photoacoustic imaging (PAI), and acquisition of rigid-linked co-registered data for characterization of human atherosclerotic plaque. FLIM has demonstrated potential for characterization and mapping of the biochemical composition of the fibrotic cap within the superficial layer (~250 μm deep under UV excitation) and for distinguishing plaque features within this cap that have been related to plaque vulnerability [8,9]. UBM employs high-frequency ultrasonic transducers (>40 MHz) that enable imaging of plaque microanatomy and morphology with high resolution (~50 μm) and penetration depth up to 4-5 mm [10]. UBM is applied to intravascular setting via IVUS rotational catheter. IVUS systems operating at frequencies greater than 40 MHz have been used in patients for the analysis of arterial wall morphology [11]. PAI can map the differences in optical absorption of various molecular constituents of tissues. More recently, PAI has been suggested as a complementary technique to IVUS and investigated as a potential modality for detection of vulnerable plaques [12]. PAI showed potential to resolve the lipid-rich from collagen-rich regions based on the distinct optical absorption signature of these components. In this context, the technique reported here combining FLIM, UBM and PAI is expected to provide complementary information regarding features of atherosclerotic plaques, specifically those that are potential predictors of plaque rupture.

While this study focuses on evaluating the ability of the hybrid (optical-ultrasonic) system to record via a compact probe multimodal data by linear-scanning, the approach reported here can be used intravascularly through a modified IVUS catheter that enables rotational-scanning. Engineering efforts integrating IVUS and fiberoptics as one catheter have been previously reported [13,14].

2. Materials and Methods

The multimodal imaging device included the following components: (1) a fast-speed time-resolved fluorescence spectroscopy (TRFS) device capable of simultaneously recording fluorescence decay characteristics in multiple spectral bands and allowing for dynamic/continuous recording of fluorescence signals that could be reconstructed into FLIM images [15,16]; (2) a UBM subsystem designed for working with high-frequency single-element ultrasonic transducers; (3) a PAI subsystem sharing the electronics and the ultrasonic data acquisition pathway with the UBM subsystem and the illumination portion with the TRFS subsystem. Concurrent application of the three modalities was achieved using a hybrid imaging probe integrating coaxially a 600 μm silica optical fiber for fluorescence excitation-collection and delivery of light for PAI and a press-focused ultrasonic transducer for UBM

#146656 - $15.00 USD Received 2 May 2011; revised 14 Jul 2011; accepted 14 Jul 2011; published 19 Jul 2011

imaging and PAI signal detection [17]. Sample scanning was achieved via an XYZ-motorized stage (1 μm positioning accuracy) that permitted translation and positioning of the hybrid probe above the atherosclerotic plaque specimen. The setup allowed sequential acquisition of co-registered FLIM-UBM-PAI images. A detailed description and a complete characterization/validation of this multimodal imaging system will be reported separately (manuscript in preparation). Here, we limit ourselves to briefly describing the system specifications relevant to the current study of atherosclerotic plaques.

2.1 FLIM Subsystem

Fluorescence was induced by a pulsed nitrogen laser (337 nm, 0.7 ns) and detected via a gated MCP-PMT (180 ps rise time) and a fast digitizer (2.5 GHz bandwidth, 20 Gsamples/s). The rapid acquisition enabled 2D dynamic recording (scanning speed 0.2 mm/s) of time-resolved fluorescence from a tissue area of interest that in turn enabled the reconstruction of a set of fluorescence lifetime images in multiple spectral bands. The lifetime was defined as the 1/e decay time of the fluorescence impulse response from the tissue that was retrieved via analytical models and Laguerre deconvolution algorithms [18]. For the current studies, the fluorescence emission was acquired and analyzed for three emission bands: 390 ± 20 nm; 450 ± 23 nm; and 540 ± 25 nm. These wavelength bands are sensitive to endogenous fluorophores within the vessel walls such as collagen, elastin, and lipid components. Individual fluorescence lifetime values for each scanning line were analyzed in both spectroscopic-format (in order to determine the plaque composition at each location), and in image-format (to determine the plaque composition within a relatively larger area). In the FLIM image, the sample area for data acquisition was defined by the fluorescence excitation-collection geometry, laser repetition rate and probe scanning speed. Specifically, in the current experiment, the pixel size of the image was 82 μm in the lateral scanning direction (x), and 200 μm between frames (y). A 2D map of fluorescence lifetime of tissue was thus generated via the same device without the need of a time-gated imaging camera typically used in conventional fluorescence lifetime imaging microscopy systems [19]. The prospect of analyzing plaque composition for large areas via FLIM and determination of the extent of lipid-rich areas is important in diagnosing plaque at high-risk of rupture.

2.2 UBM Subsystem

The UBM component used a 41 MHz transducer (6 mm focal depth, 70% bandwidth, 3.75 mm aperture size) and provided ultrasound images with an axial resolution of 37 μm and lateral resolution of 65 μm [20]. Ultrasonic backscatter signals were detected by the transducer, amplified with a low noise amplifier by 35 dB, and recorded by a digitizer with a sampling rate of 400 M samples/s). Tomographic ultrasonic data were acquired by using the XYZ positioning stage at an acquisition speed in a few minutes. The dimension of the measurement cell was 0.02 (lateral, x) × 0.2 (between scanning frames, y) × 0.002 (in depth, z) mm^3. The grey scale cross-sectional UBM images with structure segmentation were analyzed at every plane of interest and correlated with the spectroscopic signals or images. An intensity calibration curve as a function of depth was measured and used to compensate the intensity variations across the focal region of the ultrasound field.

2.3 PAI Subsystem

The PAI component was developed based on minimal modification of the configuration of the FLIM-UBM system. The fiberoptic probe used for fluorescence excitation/collection was coupled to a frequency doubled pulsed Nd: YAG laser (532 nm, 10 ns, and average fluence of 10 mJ/cm^2) to induce photoacoustic effect [6]. PAI data was acquired via the UBM transducer and receiving circuit by minor modification of the acquisition software. The imaging resolution of the PAI subsystem was 50 μm and 70 μm in axial and lateral direction, respectively. Although the PAI and UBM shared the same transducer for receiving the echoes,

#146656 - $15.00 USD Received 2 May 2011; revised 14 Jul 2011; accepted 14 Jul 2011; published 19 Jul 2011

the two imaging systems had different spatial resolution. This difference was because the PAI resolution was determined not only by the transducer but also by the frequency characteristics of the photoacoustic response (affected by the absorber size and the laser pulse width [21]. The dimension of the PAI measurement cell was 0.02 (x) × 0.2 (y) × 0.004 (z) mm^3. The acquisition speed of the PAI data was 75 s/frame due to the low repetition rate (10 Hz) of the laser source. It was straightforward and feasible adding the PAI subsystem to the bimodal approach (FLIM-UBM) and transforming into a tri-modal system (FLIM-UBM-PAI) for arterial plaque characterization/diagnosis.

2.4 Tissue Samples and Histological Preparation and Analysis

Multimodal imaging was conducted in human carotid atherosclerotic plaque samples within two hours of endarterectomy. Multimodal measurements from two human carotid plaque samples were acquired. After multimodal scanning, the orientation of the tissue specimen and location of the imaged region were marked with tissue ink and the sample was fixed in 10% formalin, embedded in paraffin, and processed routinely. Four micron tissue sections were stained with hematoxylin and eosin (H&E) and a combined trichrome/elastin method (mature collagen stained blue, elastin stained black and smooth muscle cells stained red). The histological results were used as a gold standard to correlate and validate the multimodal data.

2.5 Image Processing and Co-Registration

In the integrated probe, the UBM/FLIM portions are mechanically fixed with respect to the optical component. The transformation between the two images is therefore rigid. The offset of the optical fiber from the UBM transducer was directly measured and the corresponding X and Y translations (0.5 mm and 0.1 mm respectively) were applied to the images for overlay. No rotation of one system with respect to the other is possible in the setup. The UBM and the PAI portions are also mechanically fixed with respect to each other. Therefore, for co-registering the two types of 3D data, only rigid transformation parameters needed to be estimated. We fabricated a grid phantom from carbon fibers (thickness: ~20 μm) for measuring the six parameters of the rigid transformation. The thin carbon fibers showed excellent contrast for both UBM and PAI and provided means for determining the transformation at close to the spatial resolution of both systems. The phantom was first mechanically held horizontally in water along the focal plane of the system and underwent 3D scanning by UBM and PAI. 3D image matrices of reconstructed UBM and PAI were created with appropriate voxel dimensions. Mutual information-based rigid registration [22] was then carried out between the two imaging data sets and transformation parameters (translations: 0.15, 0.9 and 0.5 mm in the X, Y and Z directions respectively, no rotational offsets) were recorded. The phantom was translated vertically for 2 mm on either side of the focal plane in steps of 250 μm and rescanned using both UBM and PAI. The task of rigid registration was repeated at each position. Only negligible differences (<10 μm) were observed in the registration parameters. The parameters determined through this process were used to generate the results shown in this paper.

3. Results

3.1 Multimodal Measurements from Ex-Vivo Carotid Plaque

A representative example was used to demonstrate the ability of the multimodal system to retrieve complementary characteristics from the atherosclerotic plaque [Fig. 1]. The transducer-fiberoptic integrated probe used for the examination is shown in Fig. 1(b). The fluorescence lifetime map acquired in three wavelength bands showed (1) the compositional changes at the lumen-surface of the plaque at specific wavelength bands, and (2) the changes of the trend of the lifetime along wavelengths for each type of composition [Fig. 1(c)–1(e)]. Both these variations were used to characterize plaque composition. For the 390 nm channel

#146656 - $15.00 USD Received 2 May 2011; revised 14 Jul 2011; accepted 14 Jul 2011; published 19 Jul 2011

[Fig. 1(c)], the average lifetime values within three regions of interest (ROI) were compared against histopathological results that are independently from the multimodal measurement. The plaque type in the cyan circle area was determined to be collagen-rich fibrotic plaque from histology. From FLIM, a longer average lifetime of 3.12 ± 0.02 ns was observed, compared with the relatively normal area (magenta circle) that exhibited relatively shorter average lifetime of 2.0 ± 0.01 ns. The area shown by the black circle had mixed composition (collagen and lipids), as indicated by histology, and showed an average lifetime of 2.48 ± 0.01 ns. The histograms of the lifetime values of the three locations are compared in Fig. 1(f). By observing the lifetime over the three wavelength bands [Fig. 1(c)–1(e)], the normal area showed a slightly increased lifetime from 2.0 ns to 2.41 ns when the wavelength increased from 390 nm to 540 nm. In comparison, a different trend in the fibrous region (cyan circle) was observed where the lifetime decreased from 3.12 ns to 2.55 ns with the increasing wavelength. UBM images for each transverse plane were acquired from the investigated region to form a fully 3D volumetric data set. Surface renderings of the UBM volume with representative orthogonal planes are shown in Fig. 1(g) and 1(h). The co-registered FLIM data was mapped on top of the UBM volume data showing the surface composition changes of the plaque [Fig. 1(i)]. In this manner, biochemical composition of the plaque surface (i.e. the vessel lumen) was characterized by FLIM, and simultaneously anatomical information of the cross section at deeper locations was reconstructed from UBM.

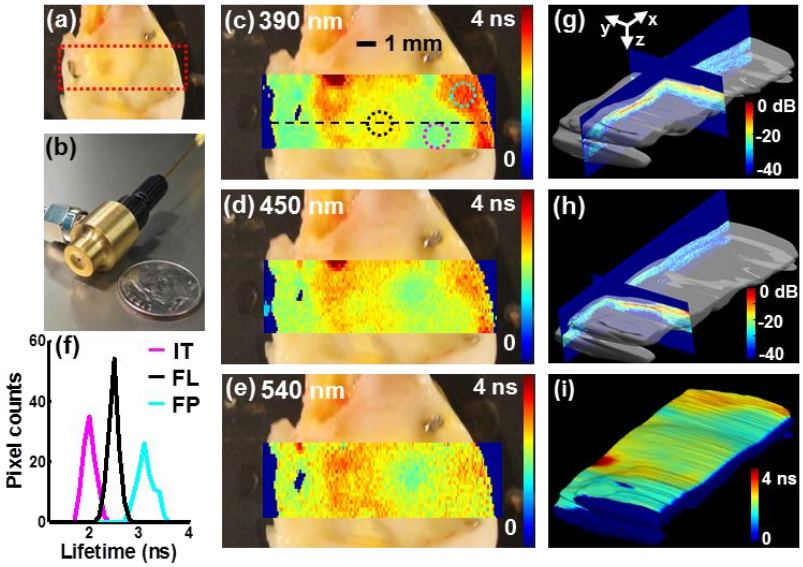

Fig. 1. Representative co-registered FLIM and UBM measurements of a human carotid plaque sample. (a) Photo of the carotid plaque sample with the imaging area outlined by the red dashed line (12.2 mm x 4 mm). (b) The combined probe integrating an ultrasonic transducer and an optical fiber. (c)-(e) FLIM images overlaid on top of the plaque photo at three different wavelengths, where the color represented average lifetime values from 0 ns to 4 ns for each pixel. Three regions were labeled in (c) and analyzed (f) Histogram of the average lifetime values at 390 nm from the three regions in (c) corresponding to three tissue types (IT: intimal thickening, FL: fibro-lipidic plaque, and FP: fibrotic plaque). (g)-(h) 3D UBM volume data from the investigated region (12.2 x 4 x 2 mm^3). Surface renderings of the UBM volume with orthogonal planes are shown with 45 dB displaying dynamics range and jet color map. (i) FLIM map at 390 nm coregistered with and overlaid onto a 3D UBM volume rendering. The minor differences in color scale between (c) and (i) are a by-product of 3D rendering. The PAI data can be displayed similarly but is not shown here to simplify the figure.

#146656 - $15.00 USD Received 2 May 2011; revised 14 Jul 2011; accepted 14 Jul 2011; published 19 Jul 2011

3.2 Correlation and Analysis of the Multimodal Measurements

In order to demonstrate the advantages provided by each modality and to show how the three modalities complemented each other, detailed analysis of the multimodal data is summarized in Fig. 2. The regions spanned by four ROIs are shown in Fig. 2(a) and the mean lifetime value was averaged over the sampling number within each region. Histopathological analysis concluded that ROI-1 corresponded to intimal thickening, ROI-2 showed fibro-lipidic plaque with calcific deposits, ROI-3 showed intimal thickening, and ROI-4 indicated fibrotic plaque [arrows in Fig. 2(e)].

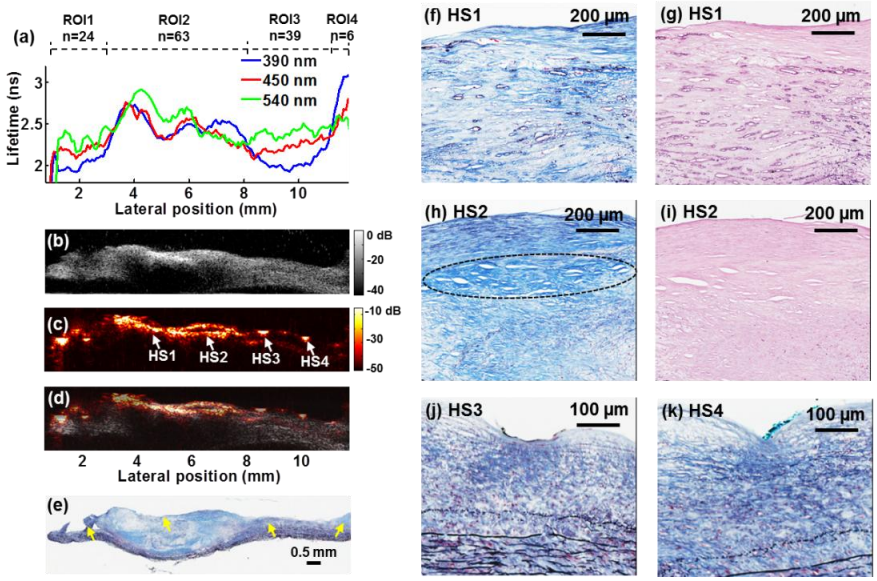

Fig. 2. Multimodal measurements and correlation analysis with histology from the scanning position indicated by the black dashed line in Fig. 1(c). (a) Plots of the average lifetime as a function of scanning position. Four ROIs were analyzed to show the changes in lumen-surface composition. (b) Transverse UBM images from the same position as (a) showed the reconstruction of the plaque structure, where an acoustic shadowing area indicated calcific deposits. (c) The PAI image provided optical absorption contrast and structural information. HS: hot spot. (d) Co-registered UBM and PAI images were fused as one combined image. (e) The corresponding trichrome stained tissue section. (f)-(k) Zoomed-in histological images of the regions labeled with HS1 to HS4 in (c): (f) HS1, trichrome staining showing fibro-lipidic plaque and calcification. Macrocalcification, and microcalcification deposits (tens of microns) were observed (dark blue circles), (g) HS1, H&E staining confirming the microcalcification, (h) HS2, trichrome staining demonstrating the fibrotic collagen-rich region (blue lines) and lipid-rich area underneath (white clefts), (i) HS2, H&E, (j) HS3, dense fibrotic knot and intimal thickening with elastin fibers (black lines) and smooth muscle cells (red), and (k) HS4, knot of collagen fibers.

In Fig. 2(a), different tissue types showed distinct average lifetime values at each channel and trends that varied as a function of wavelength. At 390 nm, the average lifetimes of the ROIs were: 2.03 ± 0.02 ns, 2.48 ± 0.02 ns, 2.09 ± 0.02 ns, and 3.0 ± 0.05 ns, respectively. The four regions were also differentiable by the trends of the average lifetime over wavelength. For example, with increasing wavelength, the lifetime increased from 2.09 to 2.40 ns (15%) for the intimal thickening composition in ROI-3 (similar trend in ROI-1) and decreased from 3.0 to 2.57 ns (17%) for the fibrotic plaque in ROI-4.

Transverse UBM grey scale images, from the same location as where the fluorescence data was acquired, demonstrated anatomical structures based on acoustic contrast [Fig. 2(b)]. The UBM image reconstructed the structure of the cross section of the plaque and showed obvious delineation of the intimal and medial layers. Thickened intima at the top of the tissue cross-

#146656 - $15.00 USD Received 2 May 2011; revised 14 Jul 2011; accepted 14 Jul 2011; published 19 Jul 2011

section corresponded to the intimal thickening regions in ROIs 1 and 3. The hyperechoic region and acoustic shadowing within the thick fibrous cap in ROI 2 indicated calcific deposits. These features were also validated by histopathological analysis of the sample.

Simultaneously acquired PAI maps provided optical absorption properties of the plaque sample [Fig. 2(c)]. The fused UBM-PAI image in Fig. 2(d) allowed the analysis of the photoacoustic response from the carotid artery sample within the anatomical delineation of the plaque reconstructed by the UBM image. The UBM-PAI image shows ultrasound echo and photoacoustic signal correlation in the fibrotic/calcific regions of the plaque. The low-amplitude photoacoustic signal presented at the plaque-media boundary was also observed in the UBM images. Within this specimen, complex compositions were observed including collagen fibers, lipids, calcification, elastin fibers, and microvessels that could all act as optical absorbers [Fig. 2(e)]. Four regions with relatively large photoacoustic signal ("hot spots" (HS1-HS4)) were delineated from Fig. 2(c) and compared against histology. Higher magnitude of photoacoustic signals appeared to come from fibrotic regions (majorly comprised of collagen fibers, HS2) or regions with calcification or microcalcification deposits (HS1) than areas with more lipids (circle area in HS2). A dense knot of collagen-rich tissue observed at HS3 and HS4 also led to an increase of overall photoacoustic response compared to the surrounding area [Fig. 2(j), 2(k)]. Correlated features retrieved from FLIM, UBM and PAI within four ROIs indicated in Fig. 3 were summarized in Table 1. The values are reported as mean ± standard error.

Table 1. Quantification of the Multimodal (FLIM-UBM-PAI) Data for Plaque Characterization (4 Locations)

Region scanning distance/ Modality	**ROI-1 1.1 – 3.0 mm**	**ROI-2 3.0 – 8.1 mm**	**ROI-3 8.1 – 11.4 mm**	**ROI-4 11.4 – 11.8 mm**
FLIM (lifetime - ns) **390 nm** **450 nm** **540 nm**	2.03 ± 0.02 2.19 ± 0.01 2.26 ± 0.04	2.48 ± 0.02 2.45 ± 0.02 2.53 ± 0.03	2.09 ± 0.02 2.24 ± 0.01 2.40 ± 0.01	3.0 ± 0.05 2.63 ± 0.05 2.57 ± 0.01
UBM: **Image evaluation** **Main features**	Delineation of intima and media layers	Hypoechoic & acoustic shadowing	Delineation of intima and media layers	Thickened fibrotic cap
PAI: **Feature evaluation**	Hot spot (artifact from sample holding pin)	High PA intensity & hot spots	Delineation of intima and media layers & hot spots	Moderate PA intensity from fibrous cap
Histology	Thin–intima elastin–rich media	Heterogenous composition (collagen, lipids, calcification) and microstructure	Thin–intima elastin–rich media	Collagen-rich area
Lifetime (ns) features in literature* [23]	Intima thickening 1.9-2.0	Fibro–lipidic plaque 2.4-2.5	Intima thickening 1.9-2.0	Fibrotic plaque 2.6-3.0
***Average fluorescence lifetime values at 390 nm.**				

A second scanning multimodal measurement from a different region as in Fig. 1 but from the same human carotid plaque was summarized in Fig. 3. This sample included three regions, histologically characterized as (from left to right): inflammation with macrophages, fibrotic-calcific, and fibrotic plaque [Fig. 3(d) arrows]. The average lifetimes in the 540 nm filter band were: 1.24 ± 0.03 ns, 1.35 ± 0.03 ns, and 1.86 ± 0.03 ns, respectively [Fig. 3(a)]. The lifetime decreased 50% for lipid-rich regions in ROI-1 compared with the fibrotic plaque in ROI-3 at this long wavelength. These results are in agreement with our earlier publication on the time-resolved fluorescence characteristics of carotid plaques [23]. The UBM image showed an increased hyperechoic region for both the calcific necrotic core under the fibrotic plaque in ROI-2 and dense collagen fibrotic region in ROI-3 [Fig. 3(b)]. The region in ROI-1 exhibited

#146656 - $15.00 USD Received 2 May 2011; revised 14 Jul 2011; accepted 14 Jul 2011; published 19 Jul 2011

a hypoechoic region corresponding to the inflammation area with macrophages. These features were also validated by histopathological analysis of the sample. The PAI image from the same location showed increased photoacoustic regions in ROI-2 and ROI-3 corresponding to the calcific and fibrotic region due to high scattering, which was consistent with the results in Fig. 2 [Fig. 3(c)]. The fused UBM and PAI image was shown in Fig. 3(d).

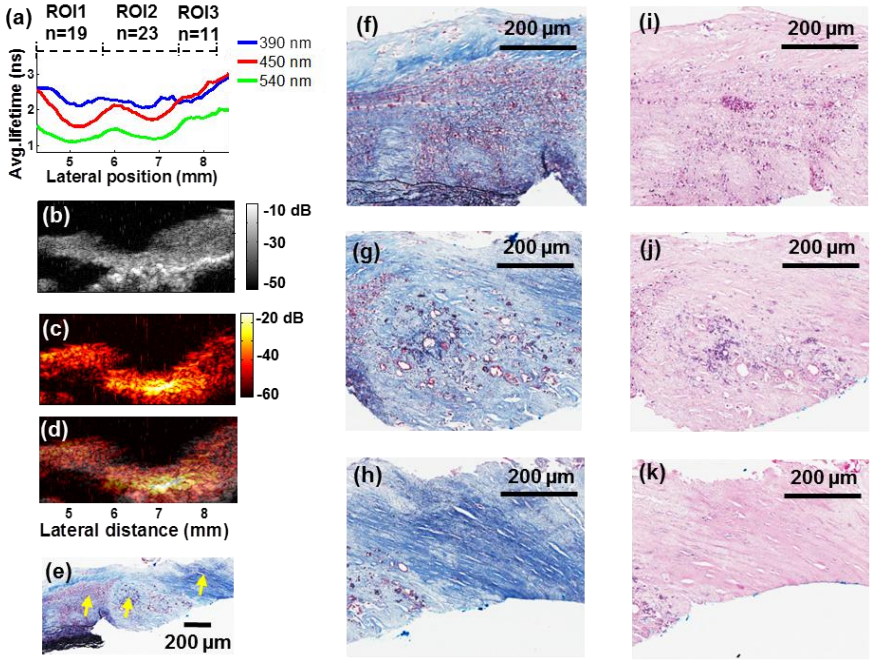

Fig. 3. Example of the multimodal measurements from a different scanning location of the carotid plaque sample and data correlation. (a) Plots of the average lifetime as a function of scanning position. Three ROIs were analyzed to show the changes in surface composition. (b) Transverse UBM images from the same position as (a) showed the reconstruction of the plaque structure, where an acoustic shadowing area indicated calcific deposits. (c) The PAI image provided optical absorption contrast. (d) Co-registered UBM and PAI images were fused as one combined image. (e) The corresponding trichrome stained tissue section. (f)-(k) Zoomed-in histological images of the regions labeled with arrows in (e): (f) and (i) inflammation\macrophages, (g) fibrotic-calcific region using the trichrome stain, (j) H&E staining confirming the presence of calcification, (h) and (k) fibrotic plaque, respectively

4. Discussion and Conclusions

The multimodal system reported here showed the ability to provide a wealth of data that is complementary for the characterization of atherosclerotic plaque. Importantly, this data can be obtained through an integrated and compact scanning probe that allows for acquisition of co-registered data from a plaque/tissue volume and display (1D, 2D, or 3D) of these data based on distinct diagnostic needs. For example (Fig. 1) 3D-UBM and PAI images acquired from a relatively large plaque volume can be co-registered with a 2D-FLIM map at the lumen-surface of this volume to provide a qualitative assessment of the distribution of distinct structural and compositional features of the plaque. In addition (Figs. 2 and 3) specific 1D (line-scanning) of fluorescence data and the corresponding 2D UBM and PAI transverse images can be also extracted from the interrogated volume. Such subset of data enables a more quantitative interpretation of fluorescence emission, correlation of tissue composition (lumen-side) with the underlying structure, and understanding the relationship between changes in fluorescent signal as a function of plaque intima thickness and/or its composition. Such analysis can be performed for every position or line of interest.

#146656 - $15.00 USD Received 2 May 2011; revised 14 Jul 2011; accepted 14 Jul 2011; published 19 Jul 2011

Fluorescence emission analysis revealed that different plaque compositions could be distinguished using lifetime values at critical emission wavelength bands. The spectroscopic parameters were sensitive to the compositional changes in ratio of plaque fluorophores: elastin, collagen, and lipids as well as the progression of atherosclerosis. For example, in Fig. 2, the lifetimes in ROI-1 and 3 were similar since the tissue type in these regions were both intimal thickening, where the fluorescence originated from the mixture of a small amount of collagen in the thin intimal layer and elastin in the medial layer as confirmed by histopathology. The lifetime in ROI-3 was slightly longer than ROI-1 due to the greater amount of collagen in ROI-3. The average lifetime of the fibrotic plaque in ROI-4 was 48% longer than the intimal thickening composition from ROI-1 because the average lifetime in ROI 4 was dominated by collagen fluorescence (3.0-4.0 ns) that has longer average lifetime than elastin (2.0-2.5 ns) [24]. Multiple features were observed in ROI-2 (rich in collagen and lipids) and the shorter average fluorescence lifetime of ROI-2 relative to the fibrotic plaque in ROI-4 denoted the contribution of the short lifetime of lipid components (0.5-1 ns) to the overall fluorescence decay [24]. The fluorescence features identified here are in agreement with previously reported extensive TRFS studies of carotid plaques [23,25] and underscore the role of fluorescence lifetime measurements in the evaluation of biochemical features in plaque intima.

UBM cannot only be used to complement the TRFS data at the surface of the plaque, but can also provide structural features at locations beyond the UV light penetration depth. Furthermore, calcification was non-fluorescent at the excitation wavelength of 337 nm and cannot be detected by TRFS only, while UBM was sensitive to calcification (e.g. Fig. 2 ROI-2) and therefore enable detection of calcified regions within plaques. The use of UBM provides a number of advantages that can be exploited in future catheter implementations. For example, the UBM image resolution can be improved by using higher frequency transducers (i.e. 60-70 MHz) with a spatial resolution of ~20 μm. At the same time, the penetration depth can still reach 3 to 4 mm as compared to the penetration depth of OCT which is usually less than 2 mm [2]. Plaque evaluation and feature extraction can be achieved not only by analyzing directly the gray scale B-mode images, but also by accessing the radiofrequency (RF) ultrasonic data which allowed for tissue composition characterization [26].

For PAI modality, a careful analysis of histological areas corresponding to distinct levels of photoacoustic signal intensity showed that the signal originating from lipid/macrophage regions was lower when compared with that originating from dense-collagen fibrous. These results are consistent with previous reports, showing the potential of PAI to resolve volumes defined by lipids/macrophages since this exhibits low optical absorption properties when compared to collagen-rich areas at the wavelength of 532 nm [12,27]. We hypothesized that the fibrotic or calcific regions were highly scattering and can result in an increase of local fluence, and therefore the magnitude of photoacoustic signals [27]. These results were observed consistently in all specimens/cross-sections [i.e. “hot spot” areas in Fig. 2(c) and Fig. 3(c)]. While additional studies (such as spectroscopic PAI) are required to confirm the role of lipids, different types of collagens, and elastin in the photoacoustic signal, the mapping of optical absorption properties in the PAI images was indicative of the physiological and pathological conditions of the tissue. As a result, a comprehensive assessment of the plaque including compositional, anatomical, and functional imaging at high resolution became possible through the combined TRFS/FLIM-UBM-PAI technique described here.

While the multimodal probe (single-fiberoptic and single-ultrasonic transducer) used in current study is not feasible for intravascular applications, current results establish the framework for future intravascular implementation. The arterial wall scanning can be achieved using a combined catheter probe through a radial scanning rather than a linear scanning as depicted here. All the knowledge generated from the UBM and PAI subsystems including image processing, feature extraction, and coregistration with fluorescence data can be translated to IVUS and intravascular photoacoustic imaging (IVPA). Specifically, the value

#146656 - $15.00 USD Received 2 May 2011; revised 14 Jul 2011; accepted 14 Jul 2011; published 19 Jul 2011

of TRFS/FLIM for continuous radial recording and synergistic radial FLIM, IVUS, and IVPA recording during a catheter pull-back in the axial direction can be demonstrated based on the expertise acquired in this study [28].

In conclusion, current results successfully demonstrate our ability to acquire rigid-linked multimodal data (FLIM, UBM, and PAI) that allows for direct data co-registration. Specifically, fluorescence lifetime images in multiple spectral bands mapped the areas occupied by varying biochemical compositions (i.e. fibrotic, lipidic, elastin-rich, etc.) and provided the opportunity for enhanced detection of critical arterial wall pathologies. Two high resolution imaging techniques (UBM and PAI) were able to provide specific anatomical and functional images of the plaques (cross-section) and overcome the limited penetration depth of the TRFS/FLIM approach. A range of signal and image processing tools were implemented and tested for the analysis of the multimodal data obtained from atherosclerotic plaques.

Acknowledgments

This work was supported by the NIH Grants R01-HL67377 and R21-EB003628. The authors also would like to acknowledge Dr. Frank Sharp and his group for providing the human atherosclerotic plaque samples, Drs. Daniel Elson, Yinghua Sun, and Ramsey D. Badawi for insightful discussions for the system design and algorithmic techniques, Longsheng Hong, and Clara E. Magyar for histology slide preparation, Hao-Chung Yang for the fabrication of transducers, Cheng Chen's help for developing data processing, and Feifei Zhou for image processing.

#146656 - $15.00 USD Received 2 May 2011; revised 14 Jul 2011; accepted 14 Jul 2011; published 19 Jul 2011